REPORT DOCUMENTATION PAGE

Form Approved
OMB No. 0704-0188

1. REPORT DATE *(DD-MM-YYYY)*	**2. REPORT TYPE**	**3. DATES COVERED** *(From - To)*
18-08-2008	Technical Paper	

4. TITLE AND SUBTITLE

A High-Order Scheme for Collisional-Ratiative and Non-Equilibrium Plasma (Preprint)

5a. CONTRACT NUMBER

5b. GRANT NUMBER

5c. PROGRAM ELEMENT NUMBER

6. AUTHOR(S)
Michael Kapper & Jean-Luc Cambier (AFRL/RZSA)

5d. PROJECT NUMBER

5e. TASK NUMBER
23040256

5f. WORK UNIT NUMBER

7. PERFORMING ORGANIZATION NAME(S) AND ADDRESS(ES)

Air Force Research Laboratory (AFMC)
AFRL/RZSA
10 E. Saturn Blvd.
Edwards AFB CA 93524-7680

8. PERFORMING ORGANIZATION REPORT NUMBER

AFRL-RZ-ED-TP-2008-361

9. SPONSORING / MONITORING AGENCY NAME(S) AND ADDRESS(ES)

Air Force Research Laboratory (AFMC)
AFRL/RZS
5 Pollux Drive
Edwards AFB CA 93524-7048

10. SPONSOR/MONITOR'S ACRONYM(S)

11. SPONSOR/MONITOR'S NUMBER(S)
AFRL-RZ-ED-TP-2008-361

12. DISTRIBUTION / AVAILABILITY STATEMENT

Approved for public release; distribution unlimited (PA #08354A).

13. SUPPLEMENTARY NOTES

For presentation at the 3rd International Workshop of Radiation of High Temperature Gases in Atmospheric Entry, Heraklion, Greece, 30 Sep – 3 Oct 2008.

14. ABSTRACT

In this paper we describe a new 3rd-order algorithm for solving the transport equations of plasma in highly non-equilibrium conditions. The plasma is described as a two-temperature, single fluid with the kinetics of collisional and radiative excitation and ionization, and reverse processes. This Collisional-Radiative model is currently limited to atomic plasma and does not include radiative transport. We describe in detail some special techniques for level grouping, scale separation of slow (transported) and fast (quasi-steady-state) level kinetics, and a non-linear transformation of the transported equations of the electronic levels to achieve the desired accuracy. The implementation and testing of the various coupling and relaxation processes are described. The fluid transport is computed using a 3rd-order variant of the MP5 monotonicity-preserving upwind advection scheme. The code is implemented in Java and parallelized through domain decomposition and hierarchical multi-threading; approach and performance are also briefly discussed. The numerical model is validated on various standard test cases, and applied to the simulation of ionizing shock front propagation in Argon. This problem shows a high sensitivity to the kinetics ladder of ionization and population of the excited states, leading to fluctuations of the location of the electron avalanche at the end of the induction zone behind the shock. We show that the collisional-radiative kinetics can reproduce the corrugations of the shock front observed in the experiment.

15. SUBJECT TERMS

16. SECURITY CLASSIFICATION OF:			**17. LIMITATION OF ABSTRACT**	**18. NUMBER OF PAGES**	**19a. NAME OF RESPONSIBLE PERSON**
					Dr. Jean-Luc Cambier
a. REPORT	**b. ABSTRACT**	**c. THIS PAGE**	SAR	20	**19b. TELEPHONE NUMBER** *(include area code)*
Unclassified	**Unclassified**	**Unclassified**			N/A

A HIGH-ORDER SCHEME FOR COLLISIONAL-RADIATIVE AND NON-EQUILIBRIUM PLASMA (PREPRINT)

Michael G. Kapper and Jean-Luc Cambier
Air Force Research Laboratory,
Edwards AFB, CA 93524 USA

August 22, 2008

Abstract

In this paper we describe a new 3rd-order algorithm for solving the transport equations of plasma in highly non-equilibrium conditions. The plasma is described as a two-temperature, single fluid with the kinetics of collisional and radiative excitation and ionization, and reverse processes. This Collisional-Radiative model is currently limited to atomic plasma and does not include radiative transport. We describe in detail some special techniques for level grouping, scale separation of slow (transported) and fast (quasi-steady-state) level kinetics, and a non-linear transformation of the transported equations of the electronic levels to achieve the desired accuracy. The implementation and testing of the various coupling and relaxation processes are described. The fluid transport is computed using a 3rd-order variant of the MP5 monotonicity-preserving upwind advection scheme. The code is implemented in Java and parallelized through domain decomposition and hierarchical multi-threading; approach and performance are also briefly discussed. The numerical model is validated on various standard test cases, and applied to the simulation of ionizing shock front propagation in Argon. This problem shows a high sensitivity to the kinetics ladder of ionization and population of the excited states, leading to fluctuations of the location of the electron avalanche at the end of the induction zone behind the shock. We show that the collisional-radiative kinetics can reproduce the corrugations of the shock front observed in the experiment.

Nomenclature

a	frozen sound speed
E	total energy density
E_e	electronic thermal energy density
E_h	heavy particle thermal energy density
$H_\circ$	specific stagnation enthalpy
M_s	shock Mach number
n	number density
p	total thermal pressure
p_e	electronic thermal pressure
p_h	heavy particle thermal pressure
T_e	electronic temperature
T_h	heavy particle temperature
$\bar{v}$	mean thermal speed
T_h	heavy particle temperature
T_e	electron temperature
$\vec{m}$	momentum density
$\vec{u}$	mass-average velocity
ρ	mass density
α	ionization fraction
ℓ	relaxation length
σ	collision cross section

1 Introduction

First introduced by Bates *et. al.* [2], Collisional-Radiative (CR) models have been extensively used in calculating population distribution of energy states as well as obtaining information about the relative significance of the various physical processes. Here we introduce a CR model coupled with a high-order convective scheme to model nonequilibrium ionization kinetics in high speed gas flows. Only the first few excited levels are included in our model which are convected as individual fluid species. It is expected that inclusion of only the first few excited levels are sufficient to capture and resolve the shock structure. With this formulation we are potentially able to determine the validity of these assumptions in various plasma regimes, and estimate their significance. This particular modeling would be useful when examining the transition of a plasma from a collisional to a radiation-dominated regime, or when looking in detail at the shock layers and relaxation regions. For the application presented here, we assume the following:

- the plasma is neutral, and all components have a single velocity (single fluid approximation).
- all components are well represented by a Maxwell-Boltzmann distribution of the velocity.
- electromagnetic effects are not considered.

In the present work, the propagation of a strong ionizing shock wave in Argon is studied, and used as a first step in the validation of our code.

2 Transport

We consider a neutral, single-fluid, two-temperature, nonequilibrium plasma. In a finite-volume framework, the hyperbolic system of equations has the form:

$$\frac{d}{dt}\int_{V(t)} Q\ dV + \oint_{S(t)} \hat{n}\cdot\mathbf{F}\ dS = \int_{V(t)} \dot{\Omega}\ dV \tag{1}$$

where

$$Q = \begin{pmatrix} \rho_1 \\ \vdots \\ \rho_n \\ \rho u \\ \rho v \\ \rho w \\ E \\ \rho\hat{s}_e \end{pmatrix}, \quad V = \begin{pmatrix} \rho_1 \\ \vdots \\ \rho_n \\ u \\ v \\ w \\ p \\ p_e \end{pmatrix}, \quad F_n = \begin{pmatrix} \rho_1 v_n \\ \vdots \\ \rho_n v_n \\ \rho u v_n + n_x p \\ \rho v v_n + n_y p \\ \rho w v_n + n_z p \\ H_\circ v_n \\ \rho\hat{s}_e v_n \end{pmatrix}, \quad \dot{\Omega} = \begin{pmatrix} \dot{\omega}_1 \\ \vdots \\ \dot{\omega}_n \\ 0 \\ 0 \\ 0 \\ \sum_s \dot{\Omega}_s^{CR} \\ \sum_s \dot{Q}_{e,s} + \dot{\Omega}_e \end{pmatrix} \tag{2}$$

with

$$E = E_h + E_e + \frac{1}{2}\rho\vec{u}\cdot\vec{u} \tag{3}$$

being the total energy density of the plasma and $H_\circ = E + p$ the stagnation enthalpy density. In order to maintain the hyperbolic property of all convected terms, the electron energy equation is formulated using the electronic entropy function $\hat{s}_e = p_e/\rho^{\gamma_e}$ (cf. [3]). The inclusion of ρ as opposed to ρ_e ensures that the function is well-defined for all ionization fractions. This leads to the following differential relations between the conservative and primitive variables:

$$dp = (\gamma_h - 1)\left[dE + \tfrac{1}{2}\vec{u}\cdot\vec{u}d\rho - \vec{u}\cdot d\vec{m} - \sum_{s\neq e}\varepsilon_s d\rho_s - \frac{\rho^{\gamma_e-1}}{\gamma_e-1}dS_e\right] + T_h\sum_{s\neq e}R_s d\rho_s + \rho^{\gamma_e-1}dS_e + (\gamma_e-\gamma_h)\frac{p_e}{\rho}d\rho \quad (4)$$

$$dE = \frac{1}{\gamma_h-1}\left[dp - T_h\sum_{s\neq e}R_s d\rho_s - dp_e\right] + \sum_{s\neq e}\varepsilon_s d\rho_s + \frac{dp_e}{\gamma_e-1} + \rho\vec{u}\cdot d\vec{u} + \tfrac{1}{2}\vec{u}\cdot\vec{u}d\rho \quad (5)$$

for which we have used the ideal gas equation of state $p = \sum \rho_s R_s T_s$ as well as

$$\gamma_h - 1 \equiv \frac{\sum\limits_{s\neq e}\rho_s R_s}{\sum\limits_{s\neq e}\rho_s c_{v,s}}. \quad (6)$$

Notice that the electron component contributes to the total plasma pressure, $p = p_h + p_e$. The electron energy equation is linear and is responsible for the heating of electrons through adiabatic compression. This final form of the electron energy convection can be derived from the reduction of the two-fluid system of equations to the single fluid system.

The term $\dot{\Omega}$ contains the source terms for the CR model. The $\dot{Q}_{\alpha,\beta}$ terms represent the energy exchange terms between the electrons and various plasma components, α, β. These terms are anti-symmetric in α, β (due to energy conservation) and their sum vanishes. The $\dot{\omega}$ are source/sink terms for specie densities due to 'chemical reactions' and radiative processes, and $\dot{\Omega}$ are the corresponding change in energy for a given plasma component due to 'chemical reactions' and radiative processes. The term 'chemical reaction' refers to any collisional process that changes the number or type of species involved. We can separate between the collisional and radiative parts, $\dot{\Omega}_s^{CR} = \dot{\Omega}_s^C + \dot{\Omega}_s^R$, and since energy conservation requires that $\sum_s \dot{\Omega}_s^C = 0$, the final sum on the R.H.S. is composed of the radiative terms only.

To this system of equations, one should add fluxes due to viscous and dissipative processes, in particular electron heat conduction, which can be a very rapid process. Our scheme also solves for this process.

The above system is solved using the operator-splitting approach under the Quasi-Steady-State (QSS) approximation. Using this approach, the convective terms are solved independently of the source terms via

$$\frac{dQ}{dt} + \frac{1}{V}\sum_s F_{n_s}A_s = 0 \quad (7)$$

which is then explicitly integrated in time using the second-order Adams-Bashforth scheme. The source terms, on the other hand, are treated implicitly, requiring a computation of a dense Jacobian matrix. Upwind fluxes at the cell interfaces are evaluated using the HLLE Riemann solver [4]. High-order spatial resolution is achieved via parabolic interpolation of the left and right states at the cell interfaces via

$$q_L = \frac{1}{6}(2\bar{q}_{j-1} + 5\bar{q}_j - \bar{q}_{j+1}) \tag{8}$$

$$q_R = \frac{1}{6}(2\bar{q}_{j+1} + 5\bar{q}_j - \bar{q}_{j-1}), \tag{9}$$

where q are the conserved quantities. The above interpolation is third-order accurate [8]. Strong nonlinear waves require limiting which modifies the left and right states according to

$$q_L \leftarrow \text{median}(q_L, \bar{q}_j, q^{MP}) \tag{10}$$

with $q^{MP} = \bar{q}_j + \text{minmod}[\bar{q}_{j+1} - \bar{q}_j, \alpha(\bar{q}_j - \bar{q}_{j-1})]$ being the monotonicity-preserving limit [7]. The value of α is taken to be 4. The right state is found from symmetry.

3 Collisional-radiative model

We have considered the following processes in our CR model,

$$Ar(i) + e \underset{F_{ji}}{\overset{C_{ij}}{\rightleftharpoons}} Ar(j) + e \tag{11}$$

$$Ar(i) + Ar(1) \underset{L_{ji}}{\overset{K_{ij}}{\rightleftharpoons}} Ar(j) + Ar(1) \tag{12}$$

$$Ar(i) + e \underset{O_i}{\overset{S_i}{\rightleftharpoons}} Ar^+ + e + e \tag{13}$$

$$Ar(i) + Ar(1) \underset{W_i}{\overset{V_i}{\rightleftharpoons}} Ar^+ + e + Ar(1) \tag{14}$$

$$Ar(i) + h\nu_{ij} \underset{A_{mn}}{\overset{(1-\Lambda_{ij})A_{ij}}{\rightleftharpoons}} Ar(j) \tag{15}$$

$$Ar(i) + h\nu \underset{R_i}{\overset{(1-\Lambda_i)R_i}{\rightleftharpoons}} Ar^+ + e \tag{16}$$

where the rate coefficients defined in [12] are summarized in table 2.

In our calculations we have considered only the excited levels of the $3p^5 4s$ manifold (cf. table 3). This implies that ionization and recombination should proceed from and to only these low-lying levels; although levels beyond this manifold are more that $1eV$ away from the ionization limit, the combination of small energy gap and large cross-section makes the ionization from these levels extremely rapid, certainly with time scales much below the time resolution needed in our computations.

Table 2: Rate coefficients for collisional-radiative model.

Rate Coefficient	Process
C_{nm}	collisional excitation by electrons
K_{nm}	collisional excitation by ground state atoms
F_{mn}	collisional de-excitation by electrons
L_{mn}	collisional de-excitation by ground state atoms
S_m, V_m	collisional ionization
O_m, W_m	three-body recombination
R_m	radiative recombination
A_{mn}	transition probability (Einstein coefficient)
Λ_{mn}	bound-bound optical escape factor
Λ_m	bound-free optical escape factor
B_m	three-body collision of metastable and ground state atoms

Table 3: Levels considered in collisional-radiative model.

i	$E(i)$	g_i	j_c	$n\ell[K]_J$
1	0	1	1.5	$3p^6$
2	11.548	5	1.5	$4s[3/2]_2$
3	11.624	3	1.5	$4s[3/2]_1$
4	11.723	1	0.5	$4s'[1/2]_0$
5	11.828	3	0.5	$4s'[1/2]_1$

Table 4: Parameters related to atom-atom processes.

i	j	β^*_{ij}
1	3	2.10×10^{-25}
1	5	4.80×10^{-25}
2	3	1.79×10^{-24}
2	4	4.80×10^{-26}
2	5	4.80×10^{-26}
3	4	4.80×10^{-26}
3	5	4.80×10^{-26}
4	5	1.79×10^{-24}

3.1 Excitation and ionization by heavy particle collisions

Since we are considering a shock propagating into a non-ionized gas, the inelastic atom-atom processes are of critical importance. Atom-atom excitation is the most important controlling process for preliminary ionization as well as the overall relaxation length. Unfortunately, very little experimental data is available for the cross sections of such processes. However, due to the relatively low energy of the flow under consideration, linear approximations are sufficient. The cross sections for excitation from ground state

$$\sigma^A_{1j}(\varepsilon) = \beta^*_{1j}(\varepsilon - \varepsilon_{ij}) \tag{17}$$

as well as for the inner $3p^5 4s$ manifold transitions

$$\sigma^A_{1j}(\varepsilon) = \beta^*_{1j}\frac{(\varepsilon - \varepsilon_{ij})}{\varepsilon^{2.26}_{ij}} \tag{18}$$

are taken from [1] with the parameter β^*_{1j} given in table 4. For direct ionization from ground state Argon we have

$$\sigma^A_{1-Ar}(\varepsilon) = 1.8 \times 10^{-25}(\varepsilon - \varepsilon_i)^{1.3}\ [m^2]. \tag{19}$$

The corresponding rate equations are

$$K_{ij} = 2\left(\frac{2k_B T_h}{\pi m_{12}}\right)^{1/2} b_{ij}(\varepsilon_{ij} + 2k_b T_h)\exp\left(-\frac{\varepsilon_{ij}}{k_B T_h}\right) \tag{20}$$

$$V_i = 2\left(\frac{2k_B T_h}{\pi m_{12}}\right)^{1/2} b_i(\varepsilon_i + 2k_b T_h)\exp\left(-\frac{\varepsilon_i}{k_B T_h}\right) \tag{21}$$

$$L_{ij} = K_{ji}(g_i/g_j)\exp(\varepsilon_{ij}/k_B T_h) \tag{22}$$

$$W_i = V_i\frac{g_i}{2g_+}\left(\frac{h^2}{2\pi m_e k_B T_e}\right)^{3/2}\exp\left(\frac{\varepsilon_i}{k_B T_h}\right) \tag{23}$$

Table 5: Parameters for the calculation of σ_{ij}^{e}. A, S, and P represent allowed, spin, and parity forbidden transitions respectively.

i	j	Transition	Parameter
1	2	S	0.111
1	3	A	0.0357, 4
1	4	S	0.0177
1	5	A	0.0813, 4
2	3	P	60
2	4	P	7
2	5	P	7
3	4	P	0.05
3	5	P	0.05
4	5	P	35
2	Ar^+	A	0.35, 4
3	Ar^+	A	0.35, 4
4	Ar^+	A	0.35, 4
5	Ar^+	A	0.35, 4

3.2 Excitation and ionization by electron impact

Excitation rates for electron impact processes are given by

$$C_{ij} = \left(\frac{8k_B T_e}{\pi m_e}\right)^{1/2} \int_{u_{ij}}^{\infty} \sigma_{ij}(u) u e^{-u}\, du \tag{24}$$

$$F_{ji} = C_{ij} \frac{g_i}{g_j} e^{\varepsilon_{ij}/k_B T_e} \tag{25}$$

where the corresponding cross sections are given by

$$\sigma_{mn} = 4\pi a_\circ^2 \begin{cases} \left(\frac{\varepsilon_1^H}{\varepsilon_{mn}}\right)^2 f_{mn}\alpha_{mn}^A U_{mn}^{-2}(U_{mn}-1) & \\ \qquad \times \ln(1.25\beta_{mn}U_{mn}) & \text{allowed} \\ \alpha_{mn}^P U_{mn}^{-1}(1-U_{mn}^{-1}) & \text{parity-forbidden} \\ \alpha_{mn}^S U_{mn}^{-3}(1-U_{mn}^{-2}) & \text{spin-forbidden} \end{cases} \tag{26}$$

The necessary parameters, $f_{mn}\alpha_{mn}^A$, α_{mn}^P, or α_{mn}^S, are given in table 5.

3.3 Photorecombination

In the absence of a third body, the energy is liberated as radiation. Photorecombination is a significant loss mechanism and plays an important role in radiative cooling. The rate for this process is given by

$$R_i = \frac{1}{2c^2 m_e k_B T_e} \frac{g_i}{g_+} \left(\frac{8k_B T_e}{\pi m_e}\right)^{1/2} \int_0^{\infty} \sigma(u)(u k_B T_e + \varepsilon_{i\infty})^2 e^{-u}\, du \tag{27}$$

where

$$h\nu = \frac{m_e v^2}{2} + \varepsilon_i \tag{28}$$

with cross sections

$$\sigma_1^P = \begin{cases} 3.5 \times 10^{-21} & \varepsilon_1 \leq h\nu \leq 2\varepsilon_H \\ 2.8 \times 10^{-20} \left(\dfrac{\varepsilon_H}{h\nu}\right)^3 & h\nu > 2\varepsilon_H \end{cases} \tag{29}$$

$$\sigma_i^P = \gamma_i(n_{pqn,\ell}) \begin{cases} 2 \times 10^{-22} & \varepsilon_i \leq h\nu \leq 0.59\varepsilon_H \\ 7.91 \times 10^{-22} \left(\dfrac{\varepsilon_i}{\varepsilon_H}\right)^{5/2} \left(\dfrac{\varepsilon_H}{h\nu}\right)^3 & h\nu > 0.59\varepsilon_H \end{cases} \tag{30}$$

3.4 Bremsstrahlung emission

Radiative cooling is taken into account via bound-free Bremsstrahlung radiation. This is given by the Kramers-Unsöld formula:

$$Q = \frac{32\pi}{3} \left(\frac{2\pi}{3m_e k_B T_e}\right)^{1/2} \frac{Z^2 e^6}{h m_e c^3} n_i n_e (h\nu_i + k_B T_e) \tag{31}$$

3.5 Elastic collisions

Elastic collisions are incorporated into the CR implicit solver as well. This strong coupling permits more accurate and stable calculations. The energy transfer between electrons and heavy particles is computed as

$$\frac{\partial E_e}{\partial t} = \frac{3}{2} n_e n_{Ar} \frac{2m_e}{m_{Ar}} (T_h - T_e) \alpha_e \tag{32}$$

where the collision rate is given by

$$\alpha_e = \frac{1}{k_B T_e^2} \left(\frac{8k_B T_e}{\pi m_e}\right)^{1/2} \int_0^\infty \sigma(\varepsilon) \varepsilon e^{-\varepsilon/k_B T_e} \, d\varepsilon. \tag{33}$$

For electron-Argon collisions, we have used the theoretical cross-sections given in table 3.5 as computed by McEachran and Stauffer [6]. The corresponding electron-Argon and electron-Argon$^+$ collision rates are given in figures 3.5 and 3.5 respectively.

4 Results and discussion

The code was applied to the case of a strong ionizing shock in Argon, in an attempt to reproduce a series of experiments by Glass & Liu [5]. The experimental cases chosen were for a shock Mach number of 14.7. The typical shock structure contains some important observable quantities which are defined here:

- M_s is the instantaneous shock Mach number.
- ℓ_* is the relaxation length, i.e. the distance from the shock front to the location of the peak ionization.

Table 6: Cross sections for e-Ar elastic collisions.

$E\ [eV]$	$\sigma \times 10^{20}\ [m^2]$
0.01	4.4679
0.03	2.9180
0.05	2.1193
0.07	1.6052
0.09	1.2481
0.13	0.7972
0.17	0.5428
0.19	0.4621
0.21	0.4002
0.23	0.3548
0.25	0.3242
0.29	0.2934
0.31	0.2898
0.32	0.2904
0.41	0.3504
0.51	0.4756
0.61	0.6403
0.71	0.8240
0.81	1.0184
0.91	1.2176
1.00	1.4002
1.50	2.4307
2.00	3.4680
3.00	5.5581
4.00	7.7317
5.00	10.0665
7.50	16.7176
10.00	22.4036

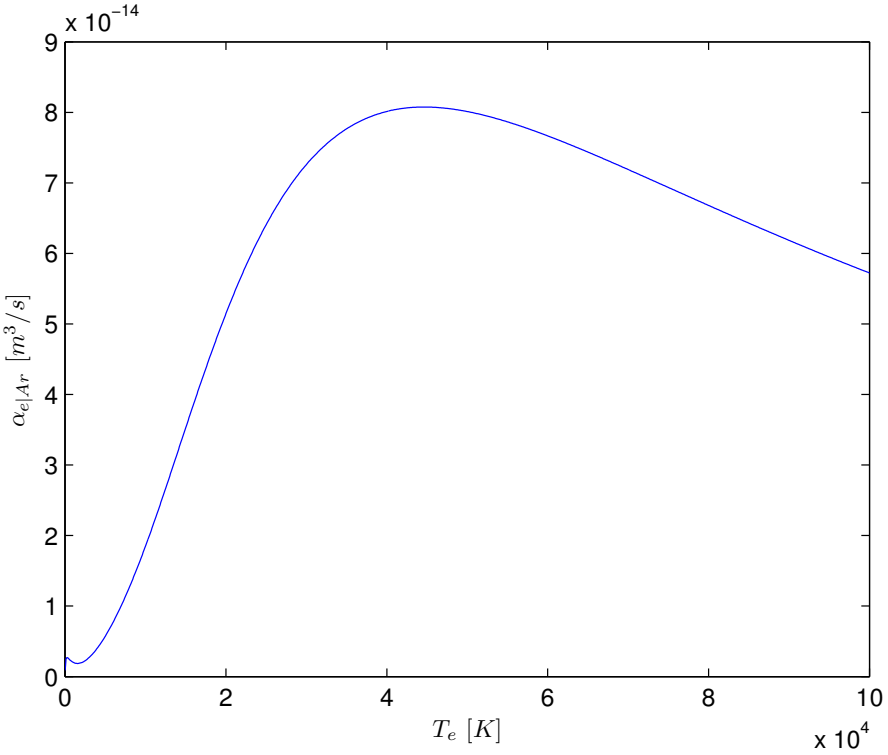

Figure 1: Electron-Ar elastic collision integral.

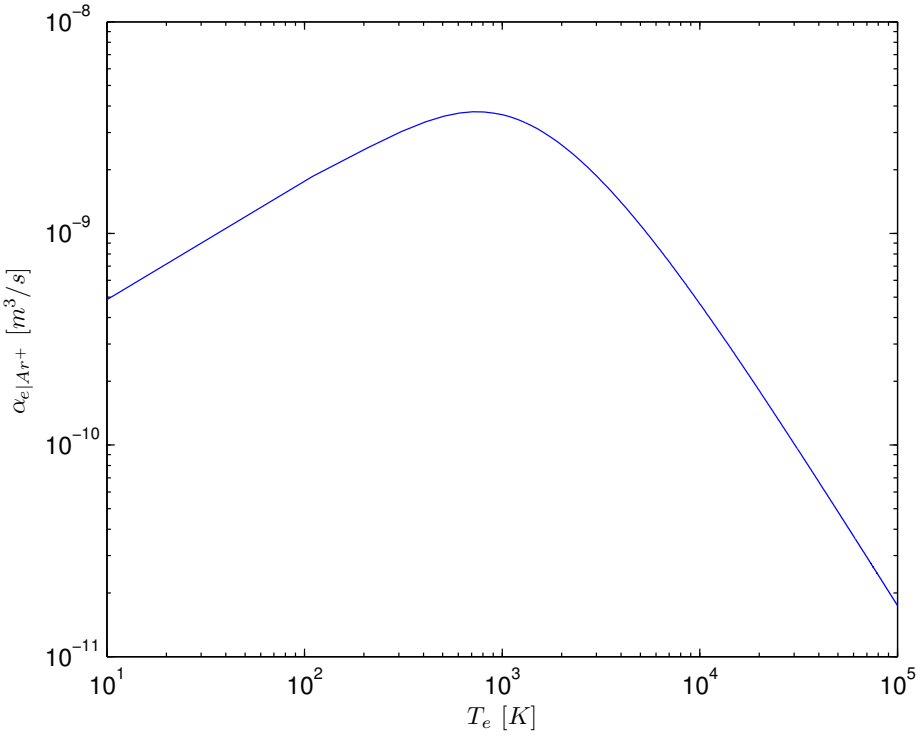

Figure 2: Electron-Ar^+ Coulomb collision integral.

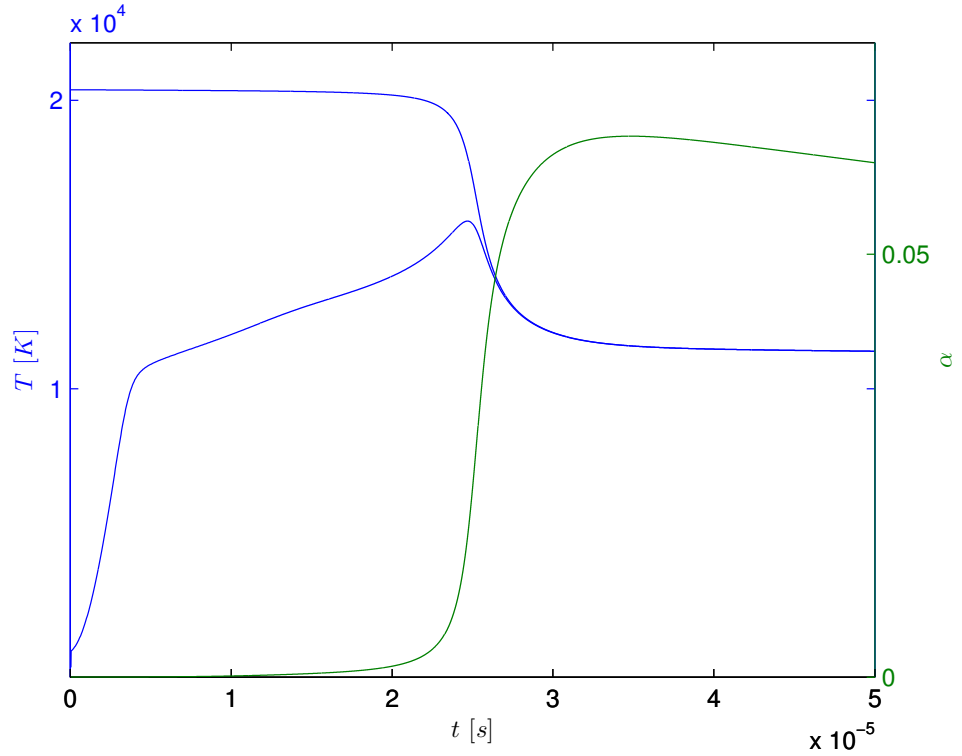

Figure 3: Results of collisional-radiative kinetics only–electron and heavy particle temperatures as well as ionization fraction.

- α_* is the peak ionization fraction.
- τ_* shock fluctuation periodicity.

Results of the stand-alone collisional-radiative kinetics solver are shown in figures 3 and 4. The simulated plasma conditions are those corresponding to a shock propagating at Mach 14.7 into an argon gas with $T_h = 300\ K$ and $p = 544\ Pa$. Evident is the initial plasma formation and thermalization between electrons and heavy particles followed by the electron avalanche and radiative cooling of the gas. The electron temperature rises rapidly to a plateau, then rises very slowly, until a maximum which corresponds to the avalanche position, then decreases until equilibrium with the heavy particles is achieved. The resulting time-dependent profile is indicative of a steady-state shock structure under the same conditions.

For coupling between the CR model and the fluid transport scheme, a shock was impulsively started by modeling a low-pressure Argon gas traveling at high velocity from left to right and reflecting off a wall at the edge of our grid system. The instantaneous measurements of the shock Mach number were accordingly transformed to the rest frame of the gas. Since the calculation is unsteady, we were able to observe the initial formation of the plasma, and its coupling to the shock front; prior to ionization, all of the energy in invested in the translational modes, and the shock speed is much greater than the final, stable value, as will be shown shortly.

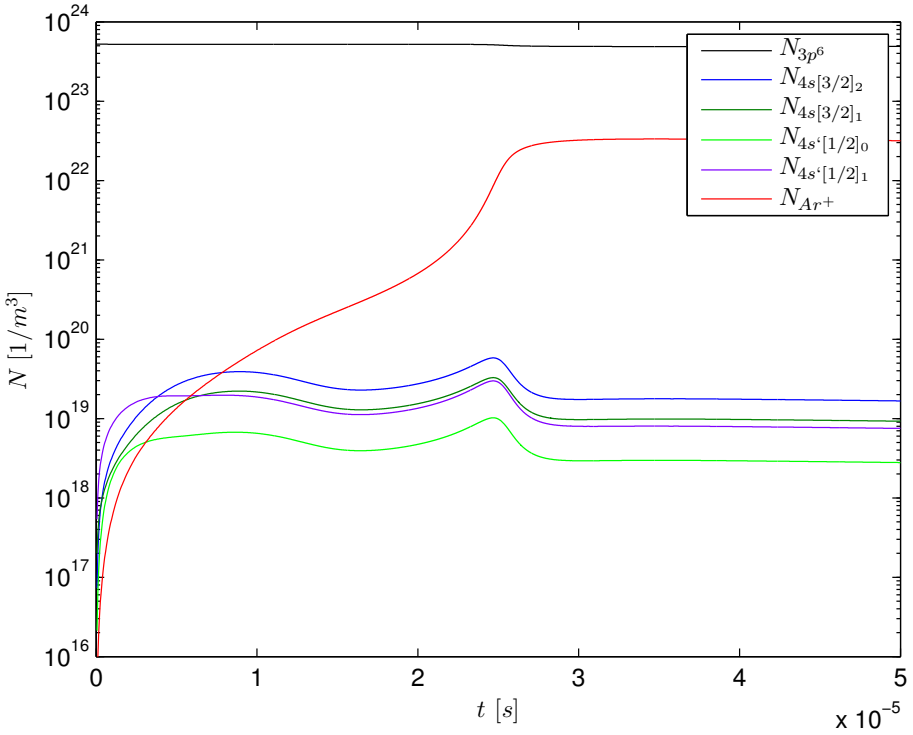

Figure 4: Results of collisional-radiative kinetics only–specie number densities.

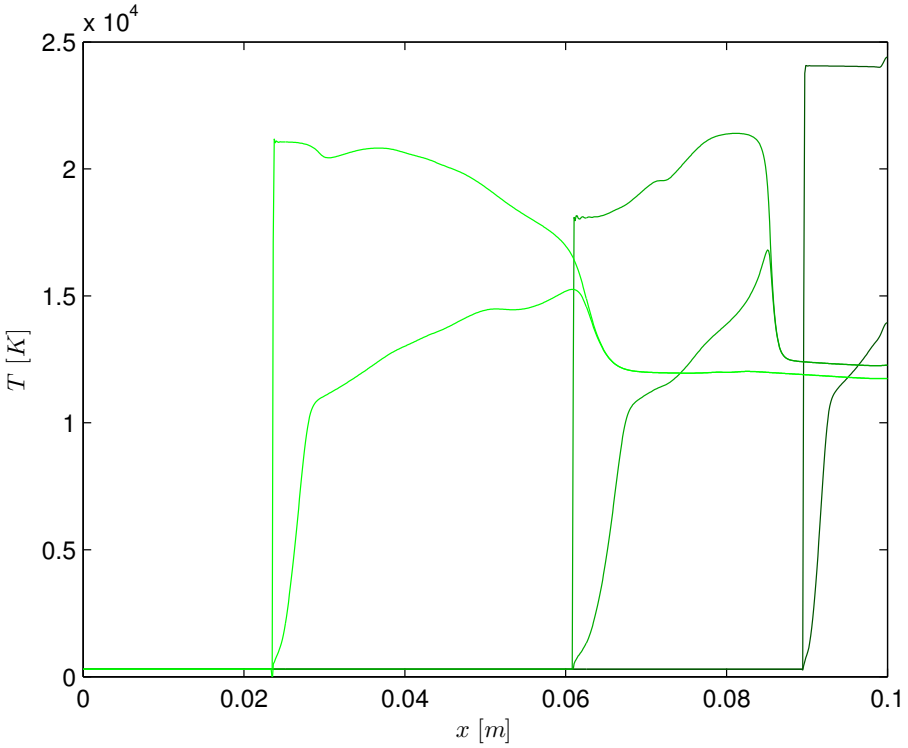

Figure 5: Temperature profiles at three different times as shock propagates away from the wall. Snapshots from right to left are taken at 8.4, 35, and 82 μsec with corresponding Mach numbers of approximately 16, 14, and 15, respectively.

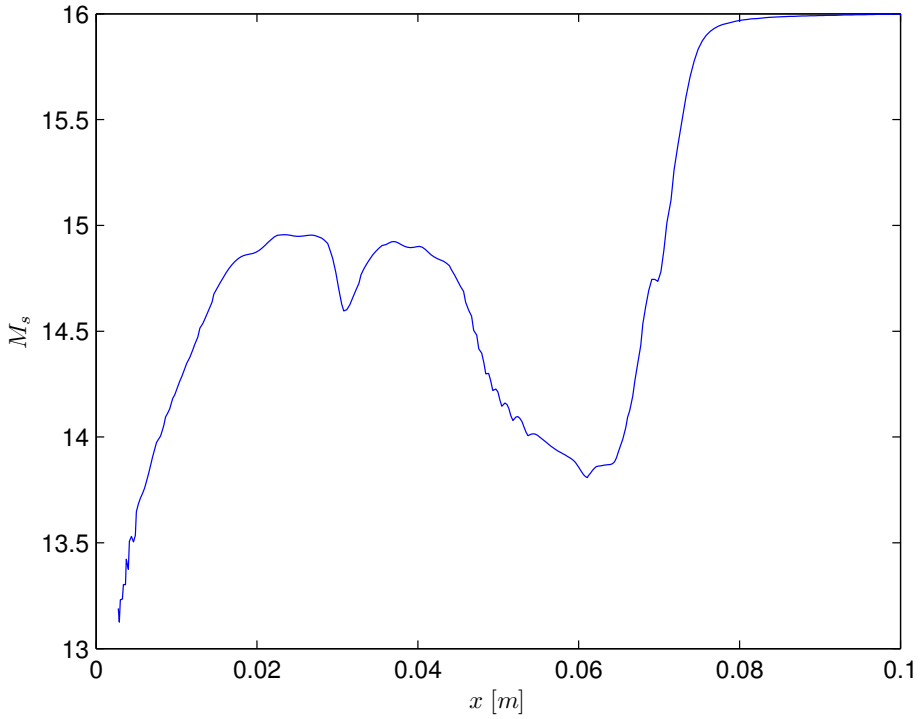

Figure 6: Shock Mach number as a function of distance.

Figure 5 shows the shock structure obtained for the case of a shock traveling with an initial Mach number of 16 into Argon with $T_h = 300\ K$ and $p = 544\ Pa$, after 3 distinct distances from the reflecting wall. These oscillations of the peak ionization, relaxation length, and shock Mach number were identified as true physical phenomena. An explanation for the coupling mechanism can be devised as follows: a pressure fluctuation travels towards the shock, and changes its velocity. As the shock strength is affected by the pressure fluctuation, the post-shock condition is slightly altered. A fluid element will go through this slightly different environment until the ionization avalanche. The overall periodicity should therefore be:

$$\tau_* \approx \ell_* \left(\frac{1}{a_2 - u_2} + \frac{1}{u_2} \right) \tag{34}$$

For $a_2 = 2890\ m/s$ and $u_2 = 3841\ m/s$, this gives a value of 24 μsec. Roughly one period of the oscillatory behavior of the shock Mach number and relaxation length is shown in figure 6. The initial shock Mach number of 16 decays to below 14 before rising again to about 15.

5 Concluding remarks

A collisional radiative database has been compiled and successfully utilized in the simulation of non-equilibrium ionizing flows in Argon. The preliminary conclusions of this study are as follows:

- The computed rates have been successfully applied to flows from $300 - 25,000K$.
- Inclusion of ground state argon with the first four levels is sufficient to accurately reproduce the correct shock structure and relaxation length.
- Fluctuations in the shock velocity, coupled to the fluctuations in the electron density at the avalanche, have been identified and investigated. These fluctuations are physical and have a definite periodic character. A coupling mechanism through the propagation of pressure waves in the relaxation region has been suggested.

The time-accurate code used here clearly is a powerful tool that can be used to eventually supplement the experimental diagnostic techniques and provide a test-bed for physical models. The computational cost is essentially dominated by the nonequilibrium kinetics. For more complex systems, notably shock layers around re-entry vehicles, the appropriate method would consist of successive approximations to the steady state with sub-cycling. The greatest advantage of the present capability is the ability to study unsteady phenomena, and this will be emphasized in the future.

6 Appendix

For completeness, we give the eigensystem for the two-temperature model.

$$R = \begin{pmatrix} 1 & \dots & 0 & y_1 & 0 & 0 & y_1 & 0 \\ \vdots & \ddots & \vdots & \vdots & \vdots & \vdots & \vdots & \vdots \\ 0 & \dots & 1 & y_n & 0 & 0 & y_n & 0 \\ u & \dots & u & u - \xi_x a & \eta_x & \zeta_x & u + \xi_x a & 0 \\ v & \dots & v & v - \xi_y a & \eta_y & \zeta_y & v + \xi_y a & 0 \\ w & \dots & w & w - \xi_z a & \eta_z & \zeta_z & w + \xi_z a & 0 \\ E_{\rho_1} & \dots & E_{\rho_n} & \mathcal{H}^- & E_{v_\eta}/\rho & E_{v_\zeta}/\rho & \mathcal{H}^+ & E_{p_e} \\ S_{e\rho_1} & \dots & S_{e\rho_n} & S_e/\rho & 0 & 0 & S_e/\rho & S_{ep_e} \end{pmatrix} \tag{35}$$

where

$$\mathcal{H}^{\pm} = \sum y_s E_{\rho_s} + \frac{\gamma_e p_e}{\rho} E_{p_e} + a^2 E_p \pm \frac{a}{\rho} E_{v_\xi}$$

and the frozen sound speed:

$$a^2 = \sum y_s P_{\rho_s} + \left[(E + p - \rho \mathbf{u} \cdot \mathbf{u}) P_E + S_e P_{S_e} \right] / \rho \tag{36}$$

$$
L = \begin{pmatrix}
1 - y_1 \frac{P_{\rho_1}}{a^2} & \cdots & -y_1 \frac{P_{\rho_n}}{a^2} & -y_1 \frac{P_{m_x}}{a^2} & -y_1 \frac{P_{m_y}}{a^2} & -y_1 \frac{P_{m_z}}{a^2} & -y_1 \frac{P_E}{a^2} & -y_1 \frac{P_{S_e}}{a^2} \\
\vdots & \ddots & \vdots & \vdots & \vdots & \vdots & \vdots & \vdots \\
-y_n \frac{P_{\rho_1}}{a^2} & \cdots & 1 - y_n \frac{P_{\rho_n}}{a^2} & -y_n \frac{P_{m_x}}{a^2} & -y_n \frac{P_{m_y}}{a^2} & -y_n \frac{P_{m_z}}{a^2} & -y_n \frac{P_E}{a^2} & -y_n \frac{P_{S_e}}{a^2} \\
\frac{P_{\rho_1} + a v_\xi}{2a^2} & \cdots & \frac{P_{\rho_n} + a v_\xi}{2a^2} & \frac{P_{m_x} - \xi_x a}{2a^2} & \frac{P_{m_y} - \xi_y a}{2a^2} & \frac{P_{m_z} - \xi_z a}{2a^2} & \frac{P_E}{2a^2} & \frac{P_{S_e}}{2a^2} \\
-v_\eta & \cdots & -v_\eta & \eta_x & \eta_y & \eta_z & 0 & 0 \\
-v_\zeta & \cdots & -v_\zeta & \zeta_x & \zeta_y & \zeta_z & 0 & 0 \\
\frac{P_{\rho_1} - a v_\xi}{2a^2} & \cdots & \frac{P_{\rho_n} - a v_\xi}{2a^2} & \frac{P_{m_x} + \xi_x a}{2a^2} & \frac{P_{m_y} + \xi_y a}{2a^2} & \frac{P_{m_z} + \xi_z a}{2a^2} & \frac{P_E}{2a^2} & \frac{P_{S_e}}{2a^2} \\
P_{e\rho_1} - \frac{\gamma_e p_e P_{\rho_1}}{\rho a^2} & \cdots & P_{e\rho_n} - \frac{\gamma_e p_e P_{\rho_n}}{\rho a^2} & -\frac{\gamma_e p_e P_{m_x}}{\rho a^2} & -\frac{\gamma_e p_e P_{m_y}}{\rho a^2} & -\frac{\gamma_e p_e P_{m_z}}{\rho a^2} & -\frac{\gamma_e p_e P_E}{\rho a^2} & P_{eS_e} - \frac{\gamma_e p_e P_{S_e}}{\rho a^2}
\end{pmatrix} \tag{37}
$$

References

[1] Anne Bourdon Arnaud Bultel, Bruno van Ootegem and Pierre Vervisch. Influence of Ar_2^+ in an argon collisional-radiative model. *Phys. Rev. E*, 65:1–16, 2002.

[2] D. R. Bates, A. E. Kingston, and R. W. P. McWhirter. Recombination between electrons and atomic ions. I: Optically thin plasmas. *Proc. R. Soc. A*, 267:297–312, 1962.

[3] S. Brassier and G. Gallice. A Roe scheme for the bi-temperature model of magneto-hydrodynamics. *Computers and Mathematics with Applications*, 41:257–267, 1998.

[4] B. Einfeldt, C.D. Munz, P.L. Roe, and B. Sjogreen. On Godunov-type methods near low densities. *J. Comput. Phys.*, 92:273–295, 1991.

[5] I.I. Glass and W.S. Liu. Effects of hydrogen impurities on shock structure and stability in ionizing monatomic gases. part1. argon. *J. Fluid Mechanics*, 84:55–77, 1997.

[6] R.P. McEachran and A.D. Stauffer. Relativistic effects in low-energy electron-argon scattering. *Aust. J. Phys.*, 50:511–524, 1997.

[7] A. Suresh and H. T. Huynh. Accurate monotonicity-preserving schemes with Runge-Kutta time stepping. *J. Comput. Phys.*, 136(1):83–99, 1997.

[8] B. van Leer. Towards the ultimate conservative difference scheme. II. monotonicity and conservation combined in a second-order scheme. *J. Comput. Phys.*, 14:361–370, 1974.

[9] B. van Leer. Towards the ultimate conservative difference scheme. III. upstream-centered finite-difference schemes for ideal compressible flow. *J. Comput. Phys.*, 23:263–275, 1977.

[10] B. van Leer. Towards the ultimate conservative difference scheme. IV. A new numerical approach to numerical convection. *J. Comput. Phys.*, 23:276–299, 1977.

[11] B. van Leer. Towards the ultimate conservative difference scheme. V. A second order sequel to Godunov's method. *J. Comput. Phys.*, 32:101–136, 1979.

[12] J. Vlček. A collisional-radiative model applicable to argon discharges over a wide range of conditions. I: Formualtion and basic data. *J. Phys. D: Appl. Phys.*, 22:623–631, 1989.